Characterization of very narrow quasi-one-dimensional quantum channels

K.-F. Berggren and G. Roos

Department of Physics and Measurement Technology, Linköping University, S581 83 Linköping, Sweden

H. van Houten

Philips Research Laboratories, 5600 JA Eindoven, The Netherlands

(Received 8 December 1987)

Narrow conducting channels are currently produced in, e.g., GaAs/Al$_x$Ga$_{1-x}$As heterostructures by means of different lithographic methods. Depending on various factors associated with the fabrication process, problems arise as to how to characterize such channels in terms of electron concentration and effective width. Here we elaborate on a simple model designed for very narrow channels in which the lateral electrostatic confinement is assumed to be a parabolic well. The confinement gives rise to one-dimensional subbands, which gradually depopulate as an increasing, perpendicular magnetic field is applied. Because of the electrostatic confinement, a plot of sublevel index n versus inverse magnetic field is generally nonlinear. This nonlinearity is used here to extract an electron concentration and width for the channel.

I. INTRODUCTION

Advances in lithographic and molecular-beam-epitaxy and metal-organic chemical-vapor-deposition techniques now make it possible to fabricate high-mobility semiconductor microstructures with quasi-one-dimensional (1D) transport behavior. Here we will focus on modulation-doped GaAs/Al$_x$Ga$_{1-x}$As heterojunctions, where electronic motion is quantum mechanically confined in two directions while being free in the third dimension, along which quasi-1D transport can occur.[1-6] As for the two-dimensional (2D) case, transverse confinement at the semiconductor interface gives rise to discrete subbands. At the usual electron concentrations [$N_e^{2D} \approx (1-5) \times 10^{15}$ m^{-2}] and low temperatures only the lowest 2D subband is occupied, which effectively removes one degree of freedom. Subsequent lateral confinement, achieved by various lithographic methods, reduces the motion in a second direction parallel to the interface. When the width of such a channel or electron waveguide is scaled down to dimensions approaching the Fermi wavelength (typically ~40–60 nm), the lateral confinement induces distinct quantized levels, separated by only a few meV or less. Therefore in this new regime of quasi-1D quantum transport a finite number of occupied 1D subbands determine the transport properties at low temperatures.

A difficulty with the characterization of narrow channels is how to determine the electron density and the width W. Ideally, a quantum-mechanical simulation based on a combined, self-consistent solution of the Schrödinger and Poisson equations for the test structure should answer this question.[7] In reality, however, this procedure is complicated by uncontrolled factors introduced by the fabrication process, such as damage-related traps and deep impurities. For example, in the split GaAs/Al$_x$Ga$_{1-x}$As heterojunction field-effect transistor (FET) of Refs. 1 and 2, a narrow conducting channel is created beneath a slit in the gate produced by electron-

beam lithography. Depending on the accelerating voltage used for the electron beam, the electron concentration in the channel may be less than that beneath the unexposed ungated regions between the gate and source and drain. The detailed mechanism behind the drop in carrier concentration is unknown. Hence, theoretical simulations are hard to implement for detailed quantitative purposes, although they give valuable general guidance. The width was therefore determined from the temperature-dependent electron-electron–interaction correction. The areal electron concentration was estimated from the period of the Shubnikov–de Haas oscillations in wide channels ($W \geq 2500$ Å). In this regime the period of the oscillations was found to be independent of W for the particular device investigated. Because of this fortunate situation, the areal electron concentration could be taken to be constant also for narrower channels in which lateral quantization sets in and causes clear deviations from a linear dependence of the Landau index on inverse magnetic field. This analysis seems to depend on rare circumstances—generally, one expects that the areal electron concentration varies with W.

Problems of the kind discussed above are also encountered in connection with mesa-etched GaAs/Al$_x$Ga$_{1-x}$As submicrometer heterostructures.[3,4] Because of sidewall depletion effects the effective width of the channel may be much smaller than the nominal width of the etched mesa. From an analysis of the weak-field negative magnetoresistance in terms of a theory for weak localization in the presence of boundary scattering, a value for the effective width may be extracted.[8,9] As mentioned above, the electron concentration in wider channels is readily obtained from Shubnikov–de Haas oscillations and the resulting value is comparable to the original material value. For narrow mesas, however, the data resemble Shubnikov–de Haas oscillations at higher fields only, but then suggest lower values for the electron concentration.

The above discussion serves to illustrate that it is not a straightforward matter to determine the width and electron concentration of very narrow quantum channels. The results depend on modeling, the accuracy of which may possibly be disputed. The purpose of the present work is to elaborate on a supplementary and elementary model which makes use of the deviations from pure Shubnikov–de Haas oscillations in narrow channels.[2] This model of magnetic depopulation of hybrid magnetoelectric 1D subbands is described in Sec. II, where it is also used to characterize the etched $GaAs/Al_xGa_{1-x}As$ mesa and the split-gate heterojunction FET mentioned above. Effects of level broadening due to elastic scattering are discussed in Sec. III. A brief summary and comments are found in Sec. IV. A preliminary report is found in Ref. 4.

II. A MODEL FOR LATERALLY CONFINED ELECTRONS IN A PERPENDICULAR MAGNETIC FIELD

Let us first consider the case of an ideal, infinite 2D electron gas in the (x,y) plane with a magnetic field B applied in the perpendicular z direction. Choosing the Landau gauge $A = B(0,x,0)$ and neglecting spin splitting because of the small g value of GaAs, one finds the Hamiltonian

$$\hat{H} = \frac{\hat{p}_x^2}{2m^*} + \frac{m^*\omega_c^2}{2}(x - x_0)^2 \tag{1}$$

for the magnetically confined motion; m^* is the effective mass, $\omega_c = |e|B/m^*$ is the cyclotron frequency, and the confining parabola is centered at $x_0 = p_y/(eB)$, where p_y is the y component of the momentum. The energy levels are

$$E_n^L = \hbar\omega_c(n + \tfrac{1}{2}), \quad n = 0,1,2,\ldots \tag{2}$$

and the eigenfunctions are of the form

$$\Psi_{n,k_y}(x,y) = \phi_n^L(x - x_0)e^{ik_y y}, \tag{3}$$

where $\phi_n^L(x)$ is the harmonic-oscillator function and $k_y = p_y/\hbar$. Ignoring lifetime broadening the density of states per unit area is

$$g_{area}(E) = \frac{|e|B}{\pi\hbar}\sum_n \delta(E - \hbar\omega_c(n + \tfrac{1}{2})). \tag{4}$$

Complete filling of n_L Landau levels therefore occurs at fields at which

$$n_L = \frac{\pi\hbar}{|e|B}N_e^{2D}, \tag{5}$$

i.e., Landau states are progressively depopulated with increasing field. If the experimentally observed minima of the Shubnikov–de Haas oscillations in the magnetoresistance are associated with the complete depopulation of Landau levels, the sheet-carrier concentration can thus be determined from the slope of a linear plot of n_L versus $1/B$.

If the system is of finite size, however, this analysis is not necessarily true because the electron states may be severely distorted by the boundaries. This would happen when the extension of an occupied Landau state exceeds the dimensions of the system. As a consequence, depopulation and Shubnikov–de Haas oscillations are modified; n_L versus $1/B$ is no longer linear.

Let us now consider the case of a narrow quantum channel in the absence of a magnetic field. If the electrostatic confinement is in the x direction and the free translational motion takes place along the y direction, the Hamiltonian for the transverse motion is

$$\hat{H} = \frac{\hat{p}_x^2}{2m^*} + V_E(x), \tag{6}$$

where $V_E(x)$ is the confining electrostatic energy term. If $V_E(x)$ is sufficiently narrow, the energy spectrum will consist of well separated, discrete sublevels E_n^0. Adding the translational motion, we have the 1D subband dispersions

$$E_n^0(k_y) = E_n^0 + \hbar^2 k_y^2/(2m^*). \tag{7}$$

The corresponding 1D density of states per unit length is, for the nth subband,

$$g_n^{1D}(E) = \frac{1}{\pi\hbar}\left[\frac{2m^*}{E - E_n^0}\right]^{1/2}\Theta(E - E_n), \tag{8}$$

where $\Theta(x) = 1$ for $x \geq 0$ and zero otherwise. Hence the total density of states per unit length is the quasi-1D expression

$$g_{Q1D}(E) = \sum_n g_n^{1D}(E). \tag{9}$$

The number of occupied subbands and the position of the Fermi level E_F follow from

$$N_e^{1D} = \frac{2}{\pi\hbar}\sum_n [2m^*(E_F - E_n^0)]^{1/2}\Theta(E_F - E_n^0)$$

$$= \sum_n N_{e,n}^{1D}, \tag{10}$$

where N_e^{1D} is the number of electrons per unit length and $N_{e,n}^{1D}$ denotes subband occupation.

If we now apply a magnetic field as above, the magnetic confinement has to be added to the Hamiltonian in Eq. (6), i.e.,

$$\hat{H} = \frac{\hat{p}_x^2}{2m^*} + V_E(x) + \frac{m^*\omega_c^2}{2}(x - x_0)^2. \tag{11}$$

The solution has the same structure as in the 1D case above, but when the electrostatic and magnetic terms are of comparable magnitude, the electron states are best described as hybrid magnetoelectric states. The magnetic term represents an additional confinement. As a consequence, the sublevel separation must increase with increasing B. Because of this diamagnetic shift a magnetic depopulation of the subbands occurs and oscillations akin to Shubnikov–de Haas oscillations appear in the magnetoresistance. The diamagnetic depopulation of the subbands is augmented by a simultaneous flattening of the

subband dispersions, which can be understood qualitatively by looking at the limit of very high fields. Then the magnetic term in Eq. (11) eventually dominates over the electrostatic confinement $V_E(x)$, and the initial parabolic subband dispersions in Eq. (7) are gradually turned into practically dispersionless Landau levels as in the 2D case.

In order to make our model quantitative, we must now specify $V_E(x)$. As emphasized in the Introduction, quantum-mechanical simulations may fail in the present context in predicting the correct electron concentration, etc., but should nevertheless give a realistic idea about the shape of the confining potential. Thus simulations for a split-gate GaAs/Al$_x$Ga$_{1-x}$As heterostructure suggest a potential which is approximately harmonic for very narrow channels.[7] For wider channels the potential shape is intermediate between that of an harmonic oscillator and a square well. In the following we will consider the case of very narrow channels by choosing

$$V_E(x) = \frac{m^* \omega_0^2}{2} x^2 ,$$ (12)

where ω_0 is a characteristic frequency defining the strength of the confinement. In zero magnetic field the sublevels are therefore $E_n^0 = \hbar\omega_0(n + \frac{1}{2})$. The choice in Eq. (12) has the attractive feature that also the Hamiltonian in Eq. (11) is exactly solvable as noted previously.[2,10–12] The total confinement is simply given by the shifted parabola

$$V(x) = \frac{m^* \omega^2}{2}(x - \bar{x}_0)^2 + \frac{\hbar^2 k_y^2}{2m^*(B)} ,$$ (13)

where $\bar{x}_0 = x_0(\omega_c/\omega)^2$, $\omega = (\omega_c^2 + \omega_0^2)^{1/2} \geq \omega_0$, and $m^*(B) = m^*(\omega/\omega_0)^2 \geq m^*$ is an effective "magnetic" mass. The corresponding eigenvalues define the hybrid magnetoelectric subbands

$$E_n(k_y) = E_n(B) + \frac{\hbar^2 k_y^2}{2m^*(B)} ,$$ (14)

where $E_n(B) = \hbar\omega(n + \frac{1}{2})$. As before, the one-particle states are

$$\psi_{n,k_y}(x,y) = \psi_n(x - \bar{x}_0)e^{ik_y y} ,$$ (15)

where ψ_n is the harmonic-oscillator function centered at $\bar{x}_0$. Since the dispersion in Eq. (14) is still parabolic, albeit with a heavier mass, Eqs. (8)–(10) remain valid if only m^* and E_n^0 are replaced by $m^*(B)$ and $E_n(B)$. The density of states thus becomes more sharply peaked in the presence of a magnetic field, leading to a greater possibility of observing structure in the magnetoresistance due to subband depopulation.

We now consider the dominant structure in the measured magnetoresistance and associate the minima with a complete depopulation of the hybrid subbands as B is increased. This assumption is reasonable since our hybrid oscillations will gradually evolve into ordinary Shubnikov–de Haas oscillations as the system is made more extended and/or the magnetic field becomes very strong. When a particular subband n is just depopulated, we have $E_F = E_n$. Hence we get from Eq. (10), after

changing m^* and E_n^0,

$$N_e^{1D} = \frac{2}{\pi}(2m^*/\hbar)^{1/2}(\omega^{3/2}/\omega_0) \sum_{\nu=1}^n \nu^{1/2} .$$ (16)

If the summation is replaced by an integration, we obtain the approximate relation

$$N_e^{1D} \approx \frac{2}{\pi}(2m^*/\hbar)^{1/2}(\omega^{3/2}/\omega_0)\frac{2}{3}n^{3/2} ,$$ (17)

which gives a fair representation of the true form, except for a small, nearly constant, overall shift. For high fields (smaller values of n) both equations give a virtually linear relation between n and $1/B$, thus resembling an ordinary n-versus-$(1/B)$ plot for Shubnikov–de Haas minima in the 2D case. This is seen by letting $\omega \rightarrow \omega_c$ in Eq. (17), i.e.,

$$n \approx \left[\frac{3\pi}{4}N_e^{1D}\omega_0 \left[\frac{\hbar}{2m^*} \right]^{1/2} \right]^{2/3} \bigg/ \omega_c ,$$ (18)

which is to be compared with Eq. (5). The slope of Eq. (18) does not, however, give the electron concentration as simply as in the 2D case. In the opposite limit of small fields (higher values of n), Eqs. (16) and (17) show a pronounced departure from linearity in n versus $1/B$ as observed in experiments. The general behavior of $n(B^{-1})$ is illustrated by Fig. 1.

Because of the similarity between Eqs. (5) and (18), it is now tempting to introduce an effective width $\tilde{W}$ for the parabolic well. If the electrons are assumed to be distributed uniformly over $\tilde{W}$, the corresponding effective 2D electron density is
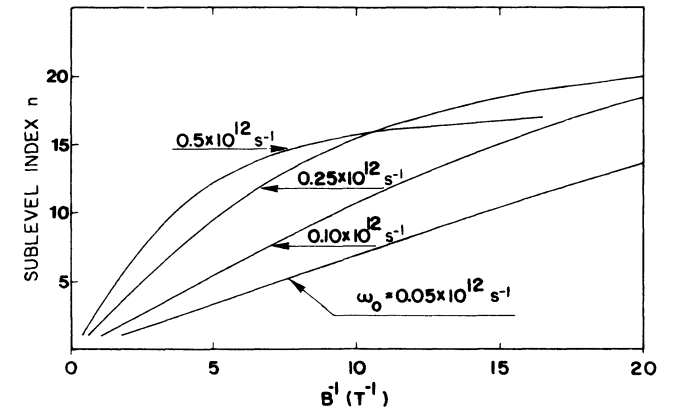
$$\tilde{N}_e^{2D} = N_e^{1D}/\tilde{W} ,$$ (19)

with

FIG. 1. Sublevel index n vs inverse magnetic field B^{-1} for parabolic confinement. The number of electrons per unit length is held constant ($N_e^{1D} = 8 \times 10^8$ m^{-1}), while the strength of the confinement is varied by means of the characteristic frequency ω_0.

$$\widetilde{W} = 2\pi (N_e^{1D})^{1/3} \left[\frac{2\hbar}{3\pi m^* \omega_0} \right]^{2/3} . \tag{20}$$

To determine N_e^{1D} and ω_0 from experiments, one may proceed in the following way. In a plot fo n versus $1/B$ the gradient of the linear region is used to find the product $(N_e^{1D}\omega_0)$ by means of Eq. (18). A fit of the full expression in Eq. (16) to the data in the nonlinear region then gives N_e^{1D} and ω_0 separately.

Figure 2(a) shows the measured magnetoresistance in an etched $Al_xGa_{1-x}As/GaAs$ mesa structure of nominal width 0.5 μm (Ref. 4). The magnetic field is perpendicular to the semiconductor interface. The oscillations, which are reproducible, are attributed to quantum fluctuations and depopulation of hybrid subbands. The latter becomes dominant at higher fields and the arrows in Fig. 2(a) indicate our assignment of subbands. At lower fields the structure associated with depopulation of subbands is
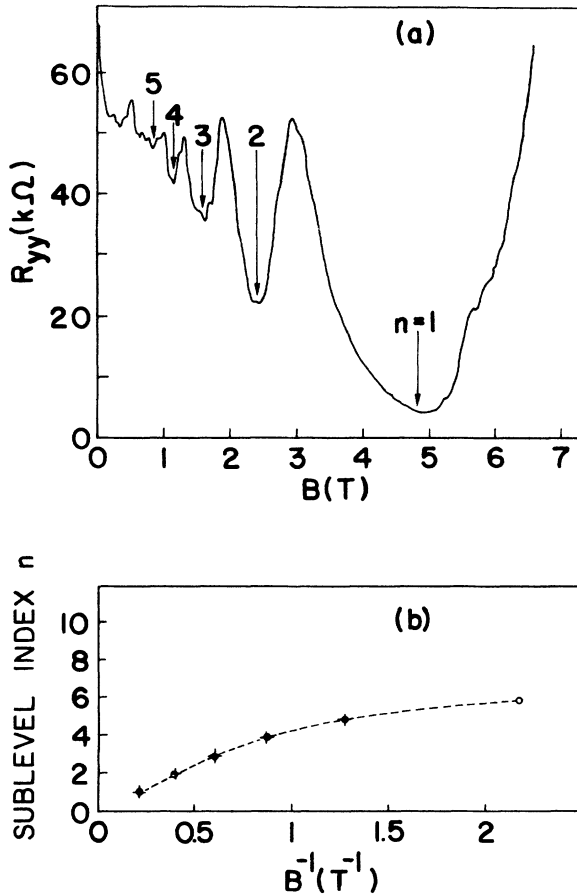

masked by quantum fluctuations. A proper assignment is therefore not feasible in this regime. Figure 2(b) shows an experimental n-versus-$(1/B)$ plot together with a theoretical fit as described above. In this way we find $N_e^{1D} = 4.27 \times 10^8$ m^{-1} and $\omega_0 = 2.31 \times 10^{12}$ s^{-1}, if a value of $0.067 m_e$ is used for the effective electron mass m^*. Furthermore we find that there are seven occupied subbands before the magnetic field is switched on. Figure 3 shows how these subbands are magnetically depopulated.

Using N_e^{1D} and ω_0 as given above, the corresponding value for the effective width is, according to Eq. (20), $\widetilde{W} = 138$ nm, i.e., much smaller than the nominal width. Equation (19) gives the effective electron concentration $\widetilde{N}_e^{2D} = 3 \times 10^{15}$ m^{-2}. Our estimate of the width is consistent with the value obtained from an analysis of the weak-field magnetoresistance,[8] namely 106 nm. This assumes that $N_e^{2D} = 2.5 \times 10^{15}$ m^{-2}, a value which is obtained from the experimental $n(1/B)$ plot by applying the 2D expression in Eq. (5) to the linear, high-field region. In this context it is illuminating also to estimate an effective width using the low-field region. Naively, one may say that deviations from linearity in n versus $1/B$ appear because the cyclotron-orbit diameter d_c becomes larger than the channel width.[4] This diameter is given by

$$d_c = 2 \left[\frac{\hbar (2n+1)}{m^* \omega_c} \right]^{1/2} . \tag{21}$$

According to Fig. 2(b), nonlinearity sets in between $B^{-1} \approx 0.6$ T^{-1} at level index $n = 3$ and $B^{-1} \approx 0.9$ T^{-1} at $n = 4$. Consequently, we find $110 < W < 145$ nm, which nicely brackets our value for $\widetilde{W}$. The classical turning points in zero field may also be used to estimate W; ω_c in Eq. (21) is then to be replaced by ω_0. With $n = 6$, the highest occupied subband, we obtain $W = 200$ nm, which is considerably larger than the previous estimates. Hence, simple arguments based on semiclassical orbit diameters should be used with some caution.

Finally, we apply the present analysis to the split-gate heterojunction discussed in the Introduction.[2] For the most narrow channel the experimental estimates are $N_e^{2D} = (1.5 \pm 0.1) \times 10^{15}$ m^{-2} and $W = 150 \pm 20$ nm. The

FIG. 2. (a) Measured magnetoresistance at 2.4 K in an etched $Al_xGa_{1-x}As/GaAs$ mesa structure of nominal width 0.5 μm (Ref. 4) (the conducting channel is along the y axis). Reproducible structure at low fields is attributed to universal conductance fluctuations. Arrows indicate our assignment of magnetic depopulation of subbands. (b) Sublevel index n vs inverse magnetic field B^{-1}. Crosses refer to minima in the measured magnetoresistance in (a) and circles to theoretical results. The dashed curve is a free interpolation to guide the eye.
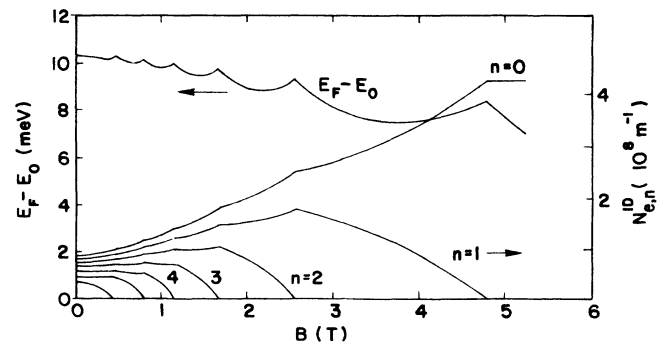

FIG. 3. Variation of Fermi energy (relative to ground-state sublevel E_0) and subband occupations $N_{e,n}^{1D}$ with magnetic field for the case in Fig. 2.

present model yields $\tilde{N}_e^{2D} = 1.57 \times 10^{15}$ m^{-2} and $\tilde{W} = 146$ nm, i.e., in good agreement with the values derived from experiments. From the onset of nonlinearity in $n(1/B)$, we have, from Eq. (21), $W \simeq 140$ nm.

III. LIFETIME BROADENING DUE TO ELASTIC SCATTERING

In the theoretical modeling above we have ignored all effects of scattering. This should be a good first approximation since we are dealing with high-mobility semiconductor structures at low temperatures. For the GaAs/Al$_x$Ga$_{1-x}$As mesa discussed in the preceding section (cf. Fig. 2), the mobility is estimated[8] to be 4 m^2/V s, which is only a factor of 2 smaller than in wide 2D electron-gas regions. Using the 2D expression for the mobility to extract a transport time τ, we estimate the level broadening $\Delta E \approx \hbar/\tau$ to be ≈ 0.5 meV. This value is to be compared with a level separation of $\Delta E_n = \hbar\omega_0 \approx 1.5$ meV. It then appears that the subbands are well resolved. Traces of subbands are easily erased, however. If, for example, the mobility would be somewhat smaller, 1–2 m^2/V s let us say, sublevels would be broadened beyond recognition by lifetime effects, and the analysis in the preceding section would be pointless. Here we will illustrate the effects of finite lifetimes on the density of states by briefly considering elastic scattering due to weak disorder. In a real system one would, of course, have to include also other scattering mechanisms, such as surface roughness, variations in the widths of the channel, etc., but the general picture we are looking for would not change drastically by such refinements.

For simplicity we let the scattering potential be represented by the random array of δ-function scatterers,

$$V_i(x,y) = a \sum_g \delta(\mathbf{r} - \mathbf{R}_g) , \qquad (22)$$

where a defines the strength of the scatterer and $\mathbf{R}_g$ random sites. Effects of lifetime broadening due to V_i in Eq. (22) have recently been examined for the case of multiply occupied 1D subbands in an infinite square well and zero magnetic field.[13] As usual in a subband situation, the lifetimes τ_n are found to differ from subband to subband and vary with energy E. Thus scattering is stronger when E is in the vicinity of a sublevel. Furthermore, τ_n is independent of k_y and, because of that, the lifetime and the transport time are identical for a particular subband in the case of δ-function scatterers. When a perpendicular magnetic field is applied as above, this picture breaks down.

To determine the lifetimes we apply the self-consistent set of equations[13]

$$\Gamma_{n,k_y}(E) = \sum_{n'} \int \frac{dk_y'}{2\pi} \overline{|\langle n,k_y | V_i | n',k_y' \rangle|^2}$$

$$\times \frac{\Gamma_{n',k_y'}(E)}{[E - E_n'(k_y')]^2 + \Gamma_{n',k_y'}^2(E)} , \qquad (23)$$

where $\Gamma_{n,k_y} = \hbar/(2\tau_{n,k_y})$ and $\overline{|\langle n,k_y | V_i | n',k_y' \rangle|^2}$ is a

configurational average. Equation (23) ignores the real part of the self-energy. For parabolic confinement, we have

$$\overline{|\langle n,k_y | V_i | n',k_y' \rangle|^2}$$

$$= a^2 N_i \int_{-\infty}^{+\infty} dx \, \psi_n^2(x - \bar{x}_0)\phi_{n'}^2(x - \bar{x}_0') , \qquad (24)$$

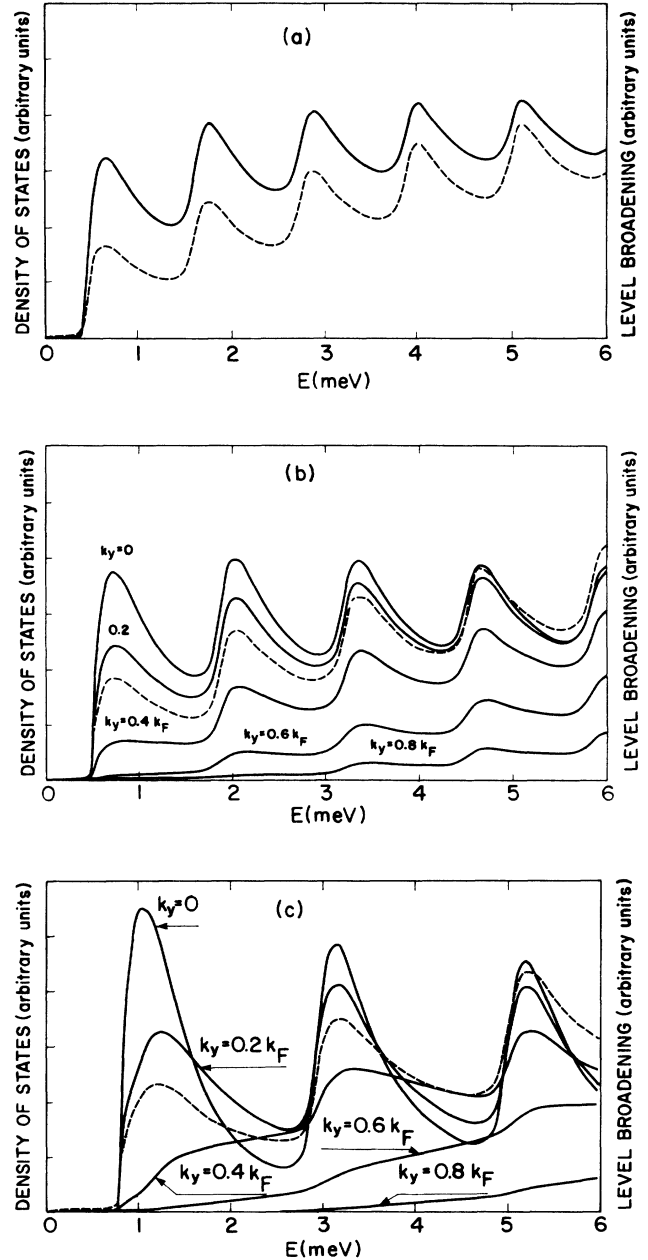where $\phi_n(x - \bar{x}_0)$ and $\phi_{n'}(x - \bar{x}_0')$ are magnetically dis-

FIG. 4. Typical behavior of total density of states broadened by finite lifetimes (dotted curves) and level broadening $\Gamma_{n,k_y}(E) = \hbar/[2\tau_{n,k_y}(E)]$ for the ground subband (solid curves). Case (a) refers to zero magnetic field; the broadening is then independent of k_y. When a magnetic field is applied, the broadening becomes strongly dependent on k_y as shown in (b) and (c), referring to $B = 0.4$ and 1 T, respectively (k_F is the Fermi wave vector for the ground subband in zero magnetic field).

placed harmonic-oscillator functions, Eq. (15), and N_i is the density of scatterers [in the derivation it is convenient to subtract a term (aN_i) from V_i]. The magnetic field acts in two ways. It leads to a general k_y dependence and a reduction of the scattering matrix elements for large momentum transfer. The last point is made clear by the explicit expression for the simplest matrix elements,

$$\overline{|\langle 0, k_y | V_i | 0, k_y' \rangle|^2} = a^2 N_i \beta e^{-\beta^2(\bar{x}_0 - \bar{x}_0')^2/2}/\sqrt{2\pi} \, , \quad (25)$$

with $\beta^2 = m^*\omega/\hbar$. The exponential damping also appears in the remaining matrix elements. Because the transverse wave functions for different wave numbers k_y become spatially separated by the magnetic field, the matrix elements for backscattering can thus decrease with increasing magnetic field. For a quantity like τ_n, this effect is counteracted by a simultaneous change in the density of states, which becomes more sharply peaked as B increases. The net result is therefore a more complex behavior of τ_n. Figure 4(a), which refers to zero magnetic field, shows a typical total density of states curve broadened by finite lifetimes τ_n. The same figure also shows $\Gamma_n(E) = \hbar/[2\tau_n(E)]$ for the ground subband. Because the scattering elements do not depend on k_y in the case of δ scatters, τ_n is only a function of energy. Figure 4(b) shows how this situation is changed when the magnetic field is turned on. Again, looking at the lowest subband only, we find that Γ_0 becomes strongly dependent on k_y. For larger values of k_y the reduction in scattering elements definitely dominates changes in the density of states. Figure 4(c), finally, shows the case of a relatively strong magnetic field. Other choices of index n result in qualitatively similar plots.

In summary, a magnetic field leads to a complex behavior of τ_n. The broadened total density of states, on the other hand, transforms in a simple way. Peaks become more widely spaced and increase in magnitude. This point is important from an experimental point of view. At zero magnetic field the subband structure may be masked by lifetime effects and/or quantum fluctuations ignored in this discussion. In the presence of a magnetic field, however, the sharpened features of the density of states should lead to a greater possibility of observing structure in the conductance owing to subband population. Although a quantity like conductance indeed reflects more than just density-of-states effects, this simple conjecture is in line with the theory of Kearney and Butcher[13] and experimental findings. However, it still remains to formulate a rigorous quantum transport theory for the present case. Such a theory would have to include finite lifetimes that depend on k_y, and, because of that, transport times which differ from the lifetimes and are specific for each subband. Although the transport theory of Smrcka, Havlova, and Ishihara[12] for a parabolically confined 2D gas is in this direction, only a single transport time is introduced.

IV. SUMMARY AND DISCUSSION

In brief, we have considered narrow quantum channels in which the transverse motion becomes quantized. Because of the confinement an applied perpendicular field leads to hybrid magnetoelectric sublevels with a spacing of levels that is different from the spacing of pure Landau levels. A plot of level index n versus inverse magnetic field therefore becomes nonlinear, particularly in the low-field region in which the cyclotron-orbit diameter exceeds the characteristic dimension of the well. This nonlinearity is used here to characterize the channel. If the confinement is assumed to be parabolic, a simple analytic result can be derived relating minima in the magnetoresistance to electron density N_e^{1D} and ω_0, the characteristic frequency of the parabolic well. N_e^{1D} and ω_0 are easily determined from a best fit to an experimental n-versus-$(1/B)$ plot. We have also shown how to find a corresponding effective width and 2D electron density that agrees well with other, independent estimates.

The parabolic model is designed for narrow channels, let us say $W \leq 2000$ Å. For wider channels it becomes numerically unreliable because the assumption of a parabolic confinement is then less realistic. Instead, one should think of a potential that flattens in the central region. However, the mechanism behind magnetic depopulation of hybrid subbands in such a potential would be the same as for the parabolic well. A drawback is that one generally would have to resort to a numerical solution of the Schrödinger equation rather than the simple analytic treatment available for the present model. For wide channels the flat region of the potential dominates and for this reason the detailed form of the confining walls matters less. In this case the problem could be simplified to a particle in an infinitely deep rectangular well plus magnetic field. Approximate, analytic solutions[14] for this situation could prove useful in the present context.

Effects of lifetime broadening have been considered briefly in Sec. III. For random δ-function scatterers it is shown that the lifetimes become strongly k_y dependent when a perpendicular magnetic field is applied. The reason is that transverse wave functions for different k_y values become spatially separated. Matrix elements for backscattering are therefore exponentially reduced. At the same time peaks in the density of states become more sharply peaked and the separation of sublevels is diamagnetically increased. This enhances the possibility of observing structure associated with magnetic depopulation of subbands.

The magnetic separation of the transverse wave functions $\psi_n(x - \bar{x}_0)$ may have profound consequences. Thus a perpendicular magnetic field causes a charge redistribution, which is equal and opposite between states k_y and $-k_y$. In the absence of current no Hall voltage is measured because there is no net movement of the "center of charge." A current flowing along the channel can be regarded as a displacement of the initial Fermi distributions centered at $k_y = 0$. This breaks the symmetry for states close to the Fermi wave vectors. Hence, if a current flows there is a net rearrangement of charge from one side of the channel to the other; consequently, a Hall voltage exists between opposite Hall probes. In the parabolic well the displacement $\bar{x}_0$ of the transverse wave functions is, however, smaller than in very wide channels in which the displacement is x_0. This difference becomes

more pronounced in weak fields. Consequently, one should expect anomalies in the Hall voltage for narrow channels in that limit. One would also expect that such anomalies grow stronger with decreasing width, and that they depend on the net current that flows along the channel, since a stronger current, for example, causes more charge to be redistributed across the channel. These features are not specific to the parabolic well, but are derived from strong confinement in general. Recently, there have been reports on the anomalous behavior of R_{xy} in narrow channels and weak magnetic fields.[6,15] Although suggestive, we find it premature to tie the present considerations to the observed anomalies.

[1]T. J. Thornton, M. Pepper, H. Ahmed, D. Andrews, and G. G. Davies, Phys. Rev. Lett. **56**, 1198 (1986).

[2]K. F. Berggren, T. J. Thornton, D. J. Newson, and M. Pepper, Phys. Rev. Lett. **57**, 1769 (1986).

[3]H. van Houten, B. J. van Wees, M. G. J. Heijman, and J. P. Andre, Appl. Phys. Lett. **49**, 1781 (1986).

[4]H. van Houten, B. J. van Wees, J. E. Mooij, G. Roos, and K. F. Berggren, Superlattices Microstruct. **3**, 497 (1987).

[5]W. Hansen, M. Horst, J. P. Kotthaus, U. Merkt, Ch. Sikorski, and K. Ploog, Phys. Rev. Lett. **58**, 2586 (1987).

[6]G. Timp, A. M. Chang, P. Mankiewich, R. Behringer, J. E. Cunningham, T. Y. Chang, and R. E. Howard, Phys. Rev. Lett. **59**, 732 (1987).

[7]S. E. Laux, D. J. Frank, and F. Stern, Surf. Sci. **196**, 101 (1988).

[8]H. van Houten, C. W. J. Beenakker, B. J. van Wees, and J. E. Mooij, Surf. Sci. **196**, 144 (1988).

[9]C. W. J. Beenakker and H. van Houten, Phys. Rev. B (to be published).

[10]J. C. Maan, in *Two-Dimensional Systems, Heterostructures and Superlattices,* edited by G. Bauer, F. Kuchar, and H. Heinrich (Springer, Berlin, 1984), p. 183.

[11]S. B. Kaplan and A. C. Warren, Phys. Rev. B **34**, 1346 (1986).

[12]L. Smrcka, H. Havlova, and A. Isihara, J. Phys. C **12**, L457 (1986).

[13]M. J. Kearney and P. N. Butcher, J. Phys. C **20**, 47 (1987).

[14]W. Zawadzki, Semicond. Sci. Technol. **2**, 550 (1987).

[15]M. L. Roukes, A. Scherer, S. J. Allen, Jr., H. G. Craighead, R. M. Ruthen, E. D. Beebe, and J. P. Harbison, Phys. Rev. Lett. **59**, 3011 (1987).